Engineering 31 (2023) 76–85

Contents lists available at ScienceDirect

Engineering

journal homepage: www.elsevier.com/locate/eng

Research
Material Science and Engineering—Article

Engineering Protein Coacervates into a Robust Adhesive for Real-Time Skin Healing

Ming Li [a,b,#], Baimei Liu [a,#], Wei Xu [c,*], Lai Zhao [a], Zili Wang [a], Haonan He [a], Jingjing Li [a], Fan Wang [a], Chao Ma [d,*], Kai Liu [a,b,d,e,*], Hongjie Zhang [a,b,d,e]

[a] State Key Laboratory of Rare Earth Resource Utilization, Changchun Institute of Applied Chemistry, Chinese Academy of Sciences, Changchun 130022, China
[b] School of Applied Chemistry and Engineering, University of Science and Technology of China, Hefei 230026, China
[c] Department of Orthopedics, Tongren Hospital, Shanghai Jiao Tong University School of Medicine, Shanghai 200336, China
[d] Engineering Research Center of Advanced Rare Earth Materials, Department of Chemistry, Tsinghua University, Beijing 100084, China
[e] Xiangfu Laboratory, Jiaxing 314102, China

ARTICLE INFO

Article history:
Received 19 October 2022
Revised 30 May 2023
Accepted 10 July 2023
Available online 19 September 2023

Keywords:
Biocomposite adhesive
Protein
DNA
Coacervates
Skin healing

ABSTRACT

Adhesives have attracted a great deal of attention as an advanced modality in biomedical engineering because of their unique wound management behavior. However, it is a grand challenge for current adhesive systems to achieve robust adhesion due to their tenuous interfacial bonding strength. Moreover, the absence of dynamic adaptability in conventional chemical adhesives restricts neoblasts around the wound from migrating to the site, resulting in an inferior tissue-regeneration effect. Herein, an extracellular matrix-derived biocomposite adhesive with robust adhesion and a real-time skin healing effect is well-engineered. Liquid–liquid phase separation is well-harnessed to drive the assembly of the biocomposite adhesive, with the active involvement of supramolecular interactions between chimeric protein and natural DNA, leading to a robustly reinforced adhesion performance. The bioadhesive exhibits outstanding adhesion and sealing behaviors, with a sheared adhesion strength of approximately 18 MPa, outperforming its reported counterparts. Moreover, the engineered bioderived components endow this adhesive material with biocompatibility and exceptional biological functions including the promotion of cell proliferation and migration, such that the use of this material eventually yields real-time *in situ* skin regeneration. This work opens up novel avenues for functionalized bioadhesive engineering and biomedical translations.

© 2023 THE AUTHORS. Published by Elsevier LTD on behalf of Chinese Academy of Engineering and Higher Education Press Limited Company. This is an open access article under the CC BY-NC-ND license (http://creativecommons.org/licenses/by-nc-nd/4.0/).

1. Introduction

Adhesives have emerged as an alternative to traditional wound closure tools such as sutures and staples, due to their superior flexibility, excellent handleability, and minimal secondary damage, among other features [1–3]. Ideal tissue adhesives are credited with the following features: strong adhesion, excellent biodegradability, mechanical compliance with the tissue, and compatibility with the dynamic biological environment [4,5]. However, key limitations remain concerning biomedical translations for chemically synthesized adhesives. The fabrication of such adhesives usually involves irritational processes, causing them to have potential toxicity in the wound microenvironment [6]. To overcome these challenges, diverse native biological macromolecules such as fibrins and collagens in the extracellular matrix (ECM) have been introduced into adhesives to regulate cell growth and migration and facilitate skin regeneration [7–11]. Yet, these biocomponents (e.g., fibrin sealants) contribute inferior interfacial bonding strength and cannot function *in situ* in a real-time fashion [12]. More importantly, conventional chemical adhesives lack tissue adaptability due to irreversible covalent cross-linking. This makes it difficult for these types of adhesives to meet the demands of dynamic wound healing, resulting in limited translational application [13]. Therefore, there is still an urgent need to develop robust bioadhesives for wound repair.

Inspired by sandcastle worms and mussels, versatile noncovalent supramolecular interactions such as electrostatic interactions,

* Corresponding authors.
E-mail addresses: weixu@shsmu.edu.cn (W. Xu), chaoma_chem@tsinghua.edu.cn (C. Ma), kailiu@tsinghua.edu.cn (K. Liu).
# These authors contributed equally to this manuscript.

https://doi.org/10.1016/j.eng.2023.07.013
2095-8099/© 2023 THE AUTHORS. Published by Elsevier LTD on behalf of Chinese Academy of Engineering and Higher Education Press Limited Company.
This is an open access article under the CC BY-NC-ND license (http://creativecommons.org/licenses/by-nc-nd/4.0/).

hydrogen bonding, and metal complexation are considered to be essential factors in a robust adhesion system [14–19]. Elastin-like protein (ELP) from ECM is regarded as a suitable candidate for the supramolecular assembly of biocomponent adhesives [20,21]. Repeated sequences of ELPs, $(VPGXG)_n$ (where V, P, and G are valine, proline, and glycine, respectively; n is the number of pentamer repeat units along the polypeptide chain; and X can be any amino acid except proline), have been shown to trigger complex coacervation process by alternating temperature or X species (e.g., lysine (Lys)), resulting in adhesion behavior [22–25]. Moreover, the biological nucleobases widely existing in DNA and RNA can serve as noncovalent bonding agents as well, due to their chemical tendency to form supramolecular interactions [14]. Thus, the introduction of nucleobases into adhesive systems could be a promising means of reinforcing adhesion performance. Considering its constituents and negative charge, DNA is anticipated to be able to interact with proteins through supramolecular interactions, which could lead to a strong biocomponent adhesive. Remarkably, strategies that mimic the composition of the ECM as well as the deployment of cytokines, growth factors, or novel active molecules can contribute to tissue repair [26–31]. In particular, epidermal growth factor (EGF), as a vital component of the ECM, promotes the migration and proliferation of keratinocytes and fibroblasts, and facilitates skin remodeling [32]. However, the application of EGF is restricted by its limited bioavailability and biostability [33,34]. So far, it remains a challenge regarding maintaining the biological function of EGF *in situ*. Thus, the rational design of noncovalent bonding and bioactive factors within a single system holds promise for the realization of robust tissue adhesion and real-time skin healing.

Herein, we develop a facile strategy to prepare an ECM-derived biological adhesive with outstanding adhesion performance, biocompatibility, and real-time healing effect. The adhesive was prepared via liquid–liquid phase separation driven by electrostatic complexation between chimeric EGF–ELP protein (EEP) and natural DNA. The multiple supramolecular interactions of the protein and DNA reinforce the adhesion, leading to excellent adhesion behavior on various hydrophilic and hydrophobic surfaces. In particular, the EEP–DNA bioassembly (termed "EED adhesive") exhibited remarkable performance on multiple biological tissues with a hemostasis effect. The EED adhesive showed an ultra-strong adhesion strength of approximately 18 MPa on hard substrates and an adhesion energy of about 40 $J{\cdot}m^{-2}$ on skin, surpassing currently reported bioadhesives. More strikingly, the bioderived components endow the EED adhesive with characteristic biological functions. Aside from promoting cell proliferation and migration, the EED adhesive dynamically remodeled the ECM in a real-time fashion and promoted skin regeneration *in situ*. Our strategy realizes the efficient introduction of biological components into adhesives with robust interfacial bonding, thereby providing a novel paradigm for the translation of adhesion healing combination therapy to potential clinical practice.

2. Materials and methods

2.1. Plasmid construction

pET25b(+)-ELP was constructed as described in our previous study [22]. The complementary DNA (cDNA) encoding human EGF (hEGF) (GenBank: AAA60744.1) was cloned via polymerase chain reaction (PCR), with the N-terminal primer 5′-TTTAAGAAGGAGATATACATATGAACAGTGATTCAGA-3′ and the C-terminal primer 5′-GCCCGGCCCCGCGCCCATTCGCAGTTCCCACCATTTCA-3′. The PCR product and the pET25b(+)-ELP vector linearized with NdeI were run on a 1% agarose gel in tris(hydroxymethyl)aminomethane (Tris)–acetate–ethylenediaminetetraacetic acid (EDTA) (TAE) buffer (per 1 L, 108 g Tris base, 57.1 mL glacial acetic acid, 0.05 $mol{\cdot}L^{-1}$ EDTA, pH 8.0). The objective gene band was cut out and purified using a spin column purification kit (DP209, TIANGEN, China). Afterward, the pET25b(+)-EGF–ELP vector was created by means of homologous recombination and transformed into chemically competent DH5α cells (Zomanbio, China) according to the manufacturer's protocol. Positive colonies were identified by means of colony PCR and were then verified by DNA sequencing.

2.2. Protein expression and purification

The pET25b expression vectors containing the ELP and EGF–ELP genes were transformed into chemically competent *Escherichia coli* (*E. coli*) BLR(DE3) cells (Novagen, Sigma, USA) and plated onto Luria–Bertani (LB) agar with 100 $\mu g{\cdot}mL^{-1}$ ampicillin. Single clones were inoculated in 100 mL of LB medium containing 100 $\mu g{\cdot}mL^{-1}$ ampicillin for shaking at 37 °C until the optical density at a wavelength of 600 (OD_{600}) reached 3–5. Subsequently, 16 mL of the seed culture was transferred into a 5 L shake flask containing 1 L of terrific broth medium (per 1 L, 12 g tryptone, 24 g yeast extract, 2.31 g potassium phosphate monobasic, 12.54 g potassium phosphate dibasic, 8 mL glycerol, 100 $\mu g{\cdot}mL^{-1}$ ampicillin), incubated at 37 °C and 220 $r{\cdot}min^{-1}$. When the cell OD_{600} reached 0.6–0.8, the temperature was downshifted to 28.5 °C, and protein production was induced by 100 μL of 1 $mol{\cdot}L^{-1}$ isopropyl β-*D*-1-thiogalactopyranoside (IPTG), shaken at 220 $r{\cdot}min^{-1}$ overnight before being harvested.

The cells harvested with centrifugation (6000 $r{\cdot}min^{-1}$, 10 min, 4 °C) were resuspended in lysis buffer (50 $mmol{\cdot}L^{-1}$ sodium phosphate buffer, pH 8.0, 300 $mmol{\cdot}L^{-1}$ NaCl, 20 $mmol{\cdot}L^{-1}$ imidazole) containing lysozyme (1 $mg{\cdot}mL^{-1}$) and DNA enzyme (5 $\mu g{\cdot}mL^{-1}$), broken up by means of ultrasonication at low temperature, and centrifuged (12 000 $r{\cdot}min^{-1}$, 90 min, 4 °C); the supernatant was then collected. The proteins were purified from the supernatant by means of Ni-sepharose chromatography (General Electric Company, USA), and the elution products were dialyzed to remove excess salt and then purified using cation exchange chromatography using a SP HP column (General Electric Company, USA) (SP lysis buffer: 50 $mmol{\cdot}L^{-1}$ sodium phosphate, 50 $mmol{\cdot}L^{-1}$ NaCl, pH 8.0; SP elution buffer: 50 $mmol{\cdot}L^{-1}$ sodium phosphate, 2 $mol{\cdot}L^{-1}$ NaCl, pH 8.0). After being purified using a desalting column, the proteins were processed by freeze-drying and then stored at −80 °C for further use.

2.3. Protein characterization

2.3.1. Sodium dodecyl sulfate polyacrylamide gel electrophoresis and Western blotting analysis

The purity of the protein was detected using sodium dodecyl sulfate polyacrylamide gel electrophoresis (SDS-PAGE) and Western blot (WB). In brief, the purified proteins were electrophoresed with 12% SDS-PAGE (150 V, 1 h) after thermal denaturation in protein loading buffer. The gels were stained with Coomassie brilliant blue staining solution (40% methanol, 10% glacial acetic acid, 1 $g{\cdot}L^{-1}$ brilliant blue R250), and were then observed and photographed under GenoSens 1800 (Clinx Science Instruments, China). Simultaneously, the gels obtained as described above were transferred to polyvinylidene fluoride (PVDF) membranes (100 V, 1 h). The membranes were blocked (5% bovine serum albumin in Tris-buffered saline with Tween-20) and incubated with anti-His tag primary antibodies overnight at 4 °C. Subsequently, the membranes were incubated with alkaline phosphatase-labeled secondary antibodies. A

BCIP/NBT kit (Meilunbio, China) was used to detect the alkaline phosphatase-labeled proteins.

2.3.2. Mass spectrometric analysis

For mass spectrometric (MS) analysis (autoflex III, matrix-assisted laser desorption ionization–time-of-flight mass spectrometry (MALDI–TOF MS), Bruker, Germany), the samples were dissolved in ultrapure water at 1 $mg{\cdot}mL^{-1}$.

2.4. Preparation of the protein adhesives

The lyophilized ELP protein (EP) and EEP were dissolved in deionized water with a final concentration of 100 $mg{\cdot}mL^{-1}$. In the same way, salmon sperm DNA (2000 base pairs (bp); Sigma-Aldrich, USA) solution was prepared in ultrapure water with a final concentration of 10 $mg{\cdot}mL^{-1}$ at room temperature. The solutions of protein and DNA were mixed with a 1:1 charge ratio; next, the mixture was oscillated and centrifuged for 5 min at 12 000 $r{\cdot}min^{-1}$. The supernatant was removed and the remaining mixture was lyophilized for 3–5 min to finally obtain the EP–DNA (ED) adhesive and EED adhesive. The method for fabricating the EEP–sodium dodecyl benzene sulfonate (SDBS) (EES) adhesive is essentially the same as that used in our previous research [22]. It is worth noting that none of the adhesives required freeze-drying when applied to soft tissues.

2.5. Characterization of EED adhesive

2.5.1. Thermogravimetric analysis

Thermogravimetric analysis (TGA) of the EED adhesive was performed using a TGA-Q50 system (TA Instruments, USA). Freshly prepared EED adhesive that had been cured for 24 h was measured. The samples were placed in a platinum pan in a nitrogen (N_2) atmosphere, with a heating/cooling rate of 10 $°C{\cdot}min^{-1}$ from room temperature to 800 °C.

2.5.2. Scanning electron microscopy

Morphology observation was performed using an S-4800 scanning electron microscopy (SEM; Hitachi, Japan) at 10 kV. The samples were mounted onto the specimen stubs by means of conductive double-sided adhesive tape and sputtered with gold for 30 s.

2.6. Lap shear test

A lap shear test was conducted using a Shimadzu Auto Graph AGX-Plus (Shimadzu, Japan) according to American Society for Testing and Materials (ASTM) standard F2255-05. The surface of steel/aluminum substrates were polished using 800 mesh sandpaper and washed with ultrapure water and ethanol. The ceramics/glass substrates were washed with ultrapure water and dried with clean paper before testing. After being freeze-dried for 3–5 min, the EED adhesive was coated evenly onto one substrate, which was then covered with another substrate to produce a lap shear joint with an overlap area of 5 mm × 5 mm. The substrates were cured for 24 h with a clamp at room temperature. Shear strength tests were then carried out with a stretching rate of 10 $mm{\cdot}min^{-1}$. For the soft-tissue test, porcine skin without fat, liver, and muscle were cut into rectangular blocks for the substrates and were covered with wipes to prevent the tissue from drying out. In the same way as for the previous method, the EED adhesive was coated evenly onto one substrate, and another piece of the same substrate was placed atop the former. The overlap area was around 5 mm × 8 mm. Light pressure was applied for 5–15 s to enhance adhesion. After curing at room temperature for 1.5–2.0 h, the shear strength was tested at a rate of 50 $mm{\cdot}min^{-1}$.

2.7. In vitro *biological activity test*

2.7.1. Proliferation of NIH/3T3 cells

The effects of EEP and EED adhesive on the proliferative status of NIH/3T3 cells were determined using a cell counting kit-8 (CCK8) assay (APExBIO, USA). In brief, the NIH/3T3 cells were seeded in 96-well plates at a density of 5×10^3 cells per well and incubated in a 5% carbon dioxide (CO_2) atmosphere at 37 °C for 16–20 h. The culture medium was removed and replaced with serum-free medium containing different concentrations of protein ranging from 1 $nmol{\cdot}L^{-1}$ to 1 $\mu mol{\cdot}L^{-1}$, and the blank group and control group were set up simultaneously. After 24 h, 10 μL of CCK8 was added to each well and incubated at 37 °C for 0.5–1.0 h. The absorbance was then measured at 450 nm using a microplate reader. For the protein–DNA adhesive, 4×10^3 NIH/3T3 cells per well were seeded to 96-well plates in 100 μL of Dulbecco's modified Eagle's medium (DMEM) supplemented with 5% fetal bovine serum (FBS) and 1% penicillin/streptomycin. After cell attachment, the media were replaced by serum-free media containing protein–DNA adhesive and incubated for 24 h. Then, CCK8 solution was added, and the absorbance was measured as described above. Four replicates of the experiment were performed.

2.7.2. Proliferation of human skin fibroblast (HSF) cells

First, 2×10^3 HSF cells per well were seeded in 96-well plates in DMEM (5% FBS, 1% penicillin/streptomycin). Meanwhile, 1 mg of protein–DNA adhesive was immersed in 1 mL of medium without serum at 37 °C for 24 h. The 96-well plates were incubated in 5% CO_2 at 37 °C for 16–20 h. The culture medium was then removed and replaced with adhesive extract diluted one-fold. After 24 h, CCK8 solution was added, and the absorbance was measured as described above. Relative cell activity was calculated by the following formula:

$$\text{Relative cell activity} = \frac{[A]_{\text{test}} - [A]_{\text{blank}}}{[A]_{\text{control}} - [A]_{\text{blank}}} \times 100\% \quad (1)$$

where $[A]_{\text{test}}$ is the absorbance value of the test group, $[A]_{\text{blank}}$ is the absorbance value of the blank group and $[A]_{\text{control}}$ is the absorbance value of the control group.

2.8. Cell migration assay

The NIH/3T3 cell migration capability was determined using scratch assays on a cell monolayer. Cells were seeded on 6-well plates at a density of 5×10^4 cells per well and cultured in DMEM with 10% FBS until growth was confluent. Then, cells were scratched using a sterile 10 μL pipette tip and gently washed with phosphate-buffered saline (PBS) to remove cellular debris. The NIH/3T3 cells were incubated with serum-free media containing 1 $\mu mol{\cdot}L^{-1}$ protein for 24 h. At the same time, the control group was set up. Images were acquired with an optical microscope (Nikon, Japan) and quantitatively analyzed with ImageJ software (National Institutes of Health, USA). The cell migration rate of each group was calculated as follows:

$$\text{Cell migration rate} = \frac{[\text{gap}]_{0\text{h}} - [\text{gap}]_{24\text{h}}}{[\text{gap}]_{0\text{h}}} \times 100\% \quad (2)$$

where $[\text{gap}]_{0\text{h}}$ is the initial scratch area, and $[\text{gap}]_{24\text{h}}$ is the 24 h scratch area.

2.9. Calcein–acetoxymethyl ester/propidium iodide cell stains

Samples were then processed for immersing, as described above. The NIH/3T3 cells were cultured in DMEM with 10% FBS

at a concentration of 2×10^4 cells per 20 mm dish for 16–20 h. The culture medium was removed and replaced with adhesive extract. After being incubated for 24 h, the culture medium was removed again, and each dish was washed three times with PBS. Then, 1 μL of calcein–acetoxymethyl ester (AM) (1 mg·mL^{-1}) for staining active living cells and 1 μL of propidium iodide (PI; 1 mg·mL^{-1}) for staining apoptotic cells were added, and then the mixture was incubated for 10–20 min. After being rinsed with PBS, the cells were viewed with laser scanning confocal microscopy (LSCM) (Nikon C2, Japan) at emission wavelengths of 488 nm for AM and 561 nm for PI.

2.10. Wound hemostasis in a rat model

A rat liver and kidney hemostasis model was established. Female Wistar rats were purchased from SPF (Beijing) Biotechnology Co. (China). The rats were anesthetized using isoflurane, and their abdomen and chest were disinfected with 75% alcohol. Surgery was performed on the mid-abdomen, exposing the liver and kidneys, and two identical punctures were then made by a 1 mL syringe needle. The EED adhesive was applied, and the hemostasis process of the liver and kidney was recorded by camera for evaluating the hemostasis of the adhesive.

2.11. In vitro *wound healing experiments*

2.11.1. Round-shape wound healing

The effect of the EED adhesive on wound healing was investigated using a full-thickness skin wound model in rats. First, the rats were randomly divided into four groups and anesthetized with pentobarbital sodium. After being completely anesthetized, the back areas of the rats were depilated with Veet hair removal cream (Veet, France) and then disinfected with 75% alcohol. A full-thickness 5 mm-diameter wound with a round shape was induced using one puncher on the back of each rat. An untreated rat (blank group) was used as a negative control, and a rat treated with recombinant hEGF (rhEGF) gel was used as a positive control. It should be noted that, in order to completely cover the wound, adhesive prepared with 10 mg of EEP was required. Therefore, 0.1 g of rhEGF gel was applied. Subsequently, each rat was housed individually, and the wound area images of each group were captured on days 0, 3, 7, 10, and 14. ImageJ was used to measure the wound size for quantitative analysis.

2.11.2. Histological analysis

Rats were randomly selected from every group and euthanized on days 10 and 14. Afterward, the fresh portions of the wound site were rapidly harvested and immersed in 4% paraformaldehyde. The fixed tissue samples were dehydrated with different concentrations of ethanol and finally embedded in paraffin. The samples were cut into slices of 2–4 μm thick, and the slices were fixed onto glass slides. The statistics of the thickness of new epidermis, the number of inflammatory cells, and the proportion of collagen deposition were evaluated using hematoxylin and eosin (H&E) staining and Masson's trichrome staining. All analyses were performed using ImageJ.

2.12. Ethics statement

All animal experiments were conducted in compliance with the Animal Management Rules of the People's Republic of China and with the approval of the Institutional Animal Care and Use Committee of the Animal Experiment Center of Jilin University (PZPX20180929070).

2.13. Statistical analysis

Origin 2021 (OriginLab, USA) and GraphPad Prism 8 software (GraphPad Software, USA) were used for the statistical analysis of data. All results were shown as mean ± standard deviation (SD). All quantitative results were analyzed from at least three specimens (n = 3–5). One-way or two-way analysis of variance (ANOVA) was used to generate p values to determine statistical significance ($^*p < 0.05$, $^{**}p < 0.01$, $^{***}p < 0.001$, and $^{****}p < 0.0001$).

3. Results and discussion

The preparation route and functional characterization of the EED adhesive are illustrated in Fig. 1. Derived from ECM, a chimeric protein consisting of functional EGF and elastin-like cationic polypeptide was designed and constructed using genetic engineering technology. With repeat sequences of $(VPGKG)_{72}$ (where K is lysine), EP has exhibited outstanding mechanical performance [35,36]. All proteins were expressed in *E. coli* and then purified by means of chromatography. Notably, the EEP had a high yield of 30–45 mg·L^{-1} at the shake flask level. In contrast, the single EGF expressed as inclusion bodies in *E. coli* involved cumbersome purification processes, resulting in a low protein production level. Such results are mainly attributed to the high solubility of EEP imparted by the hydrophilic EP, facilitating the purification via affinity chromatography. Both the EP and EEP had a purity of approximately 93.0%, as revealed by SDS-PAGE and WB analysis (Fig. S1 in Appendix A). The molecular weight of the EEP was identified as 42.8 kDa using MALDI–TOF MS (Fig. S2 and Table S1 in Appendix A).

To study the adhesion and pro-healing performance, the EED adhesives were fabricated by means of liquid–liquid phase separation, inspired by the complex coacervation of sandcastle worms and mussels (Figs. 1(c)–(e)). It is worth noting that the strongest ionic effect is obtained when substances with different charges are mixed at equimolar ratios of charge [37]. Therefore, the cationic protein EEP and anionic salmon sperm DNA were mixed at a 1:1 charge molar ratio of lysine to phosphate in aqueous solution. Driven by electrostatic interactions, the complex coacervate emerged as a water-insoluble phase. After centrifugation, the sticky EED condensate was acquired at the bottom of the tube (Fig. S3 in Appendix A). The ED adhesive was obtained analogously. Confirmed by optical microscopy, discrete droplets with a mean size of (3.2 ± 1.6) μm were formed in the EED coacervate solution (Fig. S4 in Appendix A). As evaluated by TGA, the moisture content of the EED adhesive decreased from 66.7% (w/w) to 8% (w/w) after curing for 24 h (Fig. S5 in Appendix A). In addition, SEM showed that the lyophilized EED adhesive had a porous structural morphology (Fig. 1(d)). These results revealed that additional porous structure of the EED adhesive was formed following the reduction of water content, and the contact area at the interface was increased, reinforcing the adhesive performance.

The EED adhesive exhibited excellent adhesion behaviors on diverse hydrophilic and hydrophobic surfaces, such as glass, aluminum (Al), ceramics, steel, plastic, polyvinyl chloride (PVC), and multiple biological tissues including liver, porcine skin, and muscle (Fig. 2). Porcine skin is well-known for its resemblant mechanical strength to human skin as a commonly biomimetic tissue material [38]. To further scrutinize the adhesion states of the EED adhesive to the skin, external stress was applied to the porcine skin, causing it to fold or twist. Intriguingly, the EED adhesive remained intact and exhibited robust cohesion even under an extreme case of bending back and forth at 180° (Fig. 2(b)).

Subsequently, a lap shear test of the EED adhesive was performed according to ASTM standard F2255-05 (Figs. 2(c)–(e);

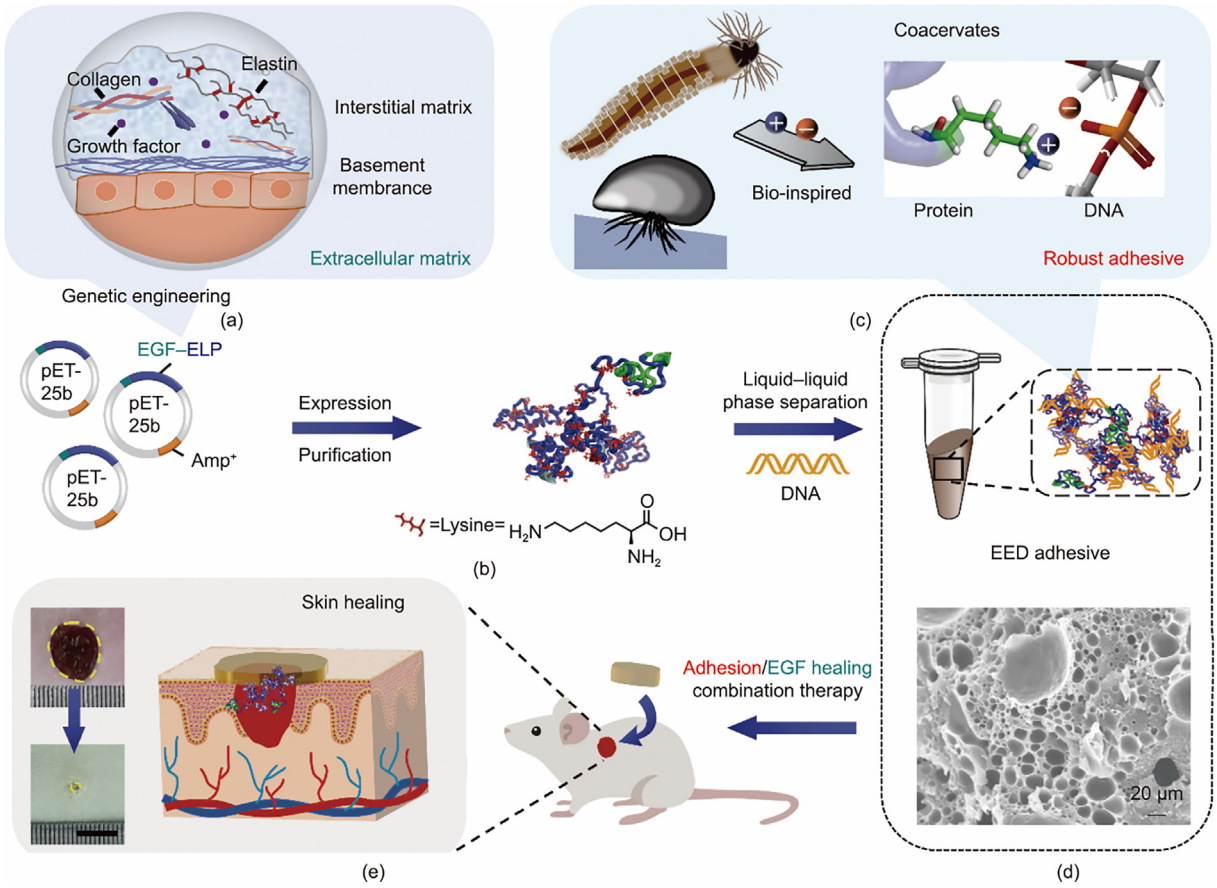

Fig. 1. Schematic illustration of the preparation and functional characterization of the EED adhesive. (a) Schematic diagram of ECM composition. Elastin and growth factor are important components of the ECM. (b) Construction and expression of the protein. Recombinant protein EEP is obtained by a fusion of EGF and ELP $(VPGKG)_{72}$ through genetic engineering technology. Amp^+: plasmid carries ampicillin resistance. (c) Preparation of the EED adhesive via bio-inspired noncovalent interactions. (d) Surface morphology of the freeze-dried EED adhesive. Inspired by mussels and sandcastle worms, the EED adhesive can be produced via liquid–liquid phase separation driven by electrostatic complexation between EEP and DNA. A porous structure in the EED adhesive was characterized using SEM. (e) Schematic representation of the EED adhesive for adhesion/EGF healing combination therapy (scale bar: 1 cm).

Figs. S6–S9 in Appendix A). The EED adhesion performance showed no temperature dependence under room temperature compared with physiologic temperature curing conditions (Fig. S6). The EED adhesive was cured under ambient conditions for 24 h; then, the typical stress–strain curves of EED adhesive on different substrates were obtained (Fig. 2(c)). The EED adhesive exhibited stronger adhesion on steel (18.9 ± 0.9) MPa than on glass (9.1 ± 0.4) MPa (Fig. 2(d)). This is presumably due to the mechanical anchoring effect of the adhesive at the contact interface [39]. Compared with glass, a polished steel surface has more grooves, which allows the EED adhesive to easily fill the cavities by wetting, squeezing, and spreading, which is conducive to superior adhesiveness after curing. Notably, the adhesion strength of the EED adhesive on steel exceeded that of commercial cyanoacrylate (11.5 ± 0.9) MPa under the same conditions (Fig. 2(d)); it also surpassed that of other reported bio-based adhesives (Table S2 in Appendix A) [23,40–44]. Compared with the single polymer network of commercial cyanoacrylate [6], the EED adhesive consists of multiple network structures formed by supramolecular interactions, such as electrostatic interactions between Lys and negative charges, hydrogen bonds in the adhesion system, and cation–π interactions in the cohesion and interface [45]. These multiple noncovalent interactions might contribute to the extraordinary cohesion and interfacial adhesion of the EED adhesive.

To assess the potential translation of the adhesives as biomedical materials, we further investigated the adhesion performance of the EED adhesive on various biological tissues (Figs. 2(e), S7(f)–(h), and S8). Notably, there was no significant difference in the adhesion properties of the non-freeze-dried treated and the lyophilized-treated adhesives under the same conditions (Fig. S9). Thus, for convenience, we preferred to utilize the EED adhesive directly without further freeze-drying in tissue applications. We also fabricated the EES adhesive as a control by replacing the DNA component with surfactant SDBS. Compared with the chemically composited EES adhesive, the EED adhesive exhibited excellent adhesion energy (Fig. 2(e)). This behavior is ascribed to the key contribution of the involved DNA components. With its unique double-stranded structure, DNA provides hydrogen bonding interactions and other supramolecular interactions as contributed by its unsaturated heterocycles, such as π–π stacking and cation–π interaction [46]. More importantly, the long double-stranded salmon sperm DNA (2000 bp) has a dense entangled strand structure, which contributes to its mechanical properties [47]. Thus, we inferred that the entanglement between ultra-long DNA chains [48] and the multi-network structure formed by the supramolecular interactions between the DNA and protein further led to the outstanding adhesion properties of the EED adhesive. In particular, the adhesive strength of the EED adhesive to porcine skin was (28.6 ± 8.0) kPa (Fig. S8) and the adhesion energy was (40.0 ± 5.3) $J \cdot m^{-2}$, exceeding those of recently reported bio-based adhesives (Table S2) [49–51].

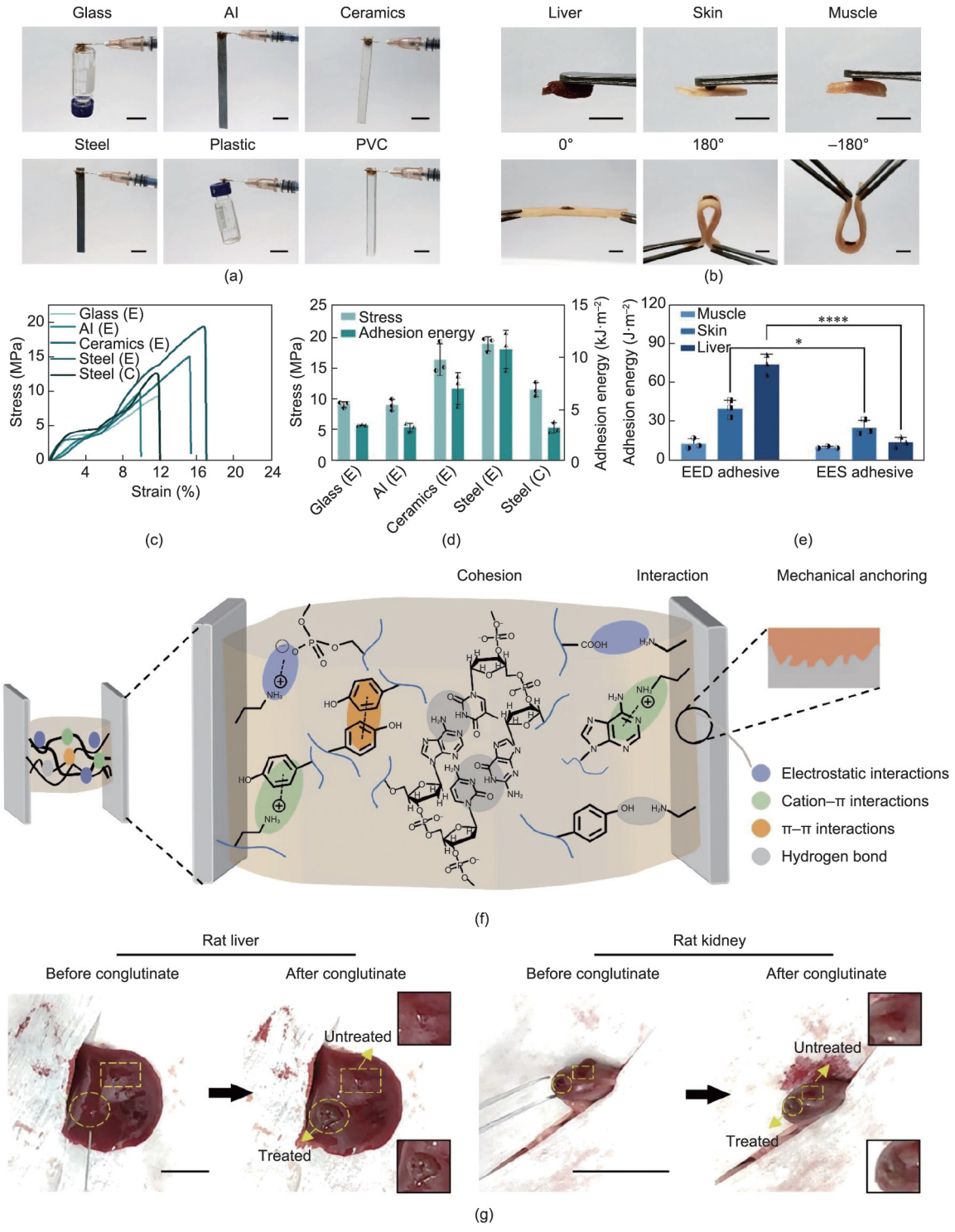

Fig. 2. Adhesion performance and mechanism of the EED adhesive on diverse substrates. (a) Adhesion of the EED adhesive on various substrates such as glass, Al, ceramics, steel, plastic, and PVC (scale bars: 1 cm). (b) Adhesion of the EED adhesive on biological tissues including liver, skin, and muscle. The EED adhesive tightly adhered to porcine skin, even when extreme external force was applied to bend the pig skin ±180° (scale bars: 1 cm). (c) Typical stress–strain curves of the EED adhesive on hard substrates. (d) Adhesion strength of the EED adhesive on different substrates. In particular, the adhesion strength of the EED adhesive on steel (~18 MPa) was higher than that of commercial cyanoacrylate (~11 MPa). Here, E represents the test of the EED adhesive, and C represents the test of cyanoacrylate. (e) Adhesion energy of the EED adhesive and the EES adhesive on muscle, porcine skin, and liver. The adhesion energy of the EED adhesive reached ~40 J·m^{-2} on porcine skin, exceeding that of the EES adhesive ($^{*}p < 0.05$ and $^{****}p < 0.0001$). (f) Illustration of the lap shear test and the adhesion mechanism of the EED adhesive on tissue. In addition to the mechanical anchoring at the interface, electrostatic interactions, cation–π, hydrogen bonding, π–π, and other interactions are important for the strong adhesions between the adhesive and the bonding surface, resulting in robust adhesive properties. (g) *In vivo* adhesion demonstration of the EED adhesive on the liver and kidney of a rat hemostasis model (scale bars: 1 cm).

Based on the experimental data, a potential adhesion mechanism of EED adhesive is proposed in Fig. 2(f). Aside from the mechanical anchoring effect, the multiple supramolecular interactions (hydrogen bonding and electrostatic, hydrophobic, and cation–π interactions, etc.) play a vital role in the robust cohesion and adhesion of the adhesive [52]. Electrostatic and hydrophobic interactions drive the

coacervation process in the cohesion part, which is similar to the coacervation of Mfp-3S in mussel adhesive plaques [53]. Moreover, the cohesion is further enhanced in our system by the hydrogen bonding of DNA and multiple interactions (e.g., π–π stacking and cation–π interactions) between the DNA and proteins [46]. In addition, the excellent interfacial adhesion benefits from hydrogen bonding interactions between amines and hydroxyl groups, cation–π interactions between positive surface charges and unsaturated heterocycles, and electrostatic interactions [14]. The reversible supramolecular interactions are believed to endow the material with a unique toughness [54], granting the EED adhesive excellent adaptability for dynamic wound healing.

Notably, the EED adhesive maintained superior underwater adhesion behavior on various substrates (e.g., steel, PVC, ceramics, and porcine skin) (Fig. S10 in Appendix A). More specifically, after being immersed in water for 5 min, the wet adhesion still remained at (17.6 ± 7.8) J·m^{-2} on skin and (14.1 ± 1.6) MPa on steel (Fig. S11 in Appendix A). This excellent wet adhesive property of the EED adhesive indicates its great potential for tissue adhesives. In addition, unlike ultraviolet (UV)-curable adhesive, which requires a relatively long time for the preparation process [55], the noncovalent binding system of the EED adhesive rapidly initiates adhesion, granting it unique merit for translation. Thus, the hemostatic efficacy of the EED adhesive was evaluated on bleeding models of rat liver and kidney (Fig. 2(g), Videos S1 and S2 in Appendix A). Two wound defect models were constructed via puncture on the same tissue, and EED adhesive was applied to one of the hemorrhaging defects. The bleeding was effectively controlled in the EED group, while significant bleeding continued in the untreated defect after 50 s. These experiments confirmed that the EED adhesive exhibits strong and effective adhesion and sealing behaviors on the complex and irregular surface of tissues.

Considering the active function of EGF, the biological activities of EEP were further explored by CCK8 assay. Initially, the NIH/3T3 cells were cultured in serum-free medium containing different concentrations of EEP, EP, and rhEGF standard. After 24 h, it was found that the cell viability of each group increased, especially at a concentration of 50 nmol·L^{-1} (Fig. 3(a)). There was no significant difference between EEP and rhEGF in terms of cell viability. This result indicated that EEP exhibited a similar capacity to promote cell proliferation as rhEGF. Such behavior might be made possible by the effective interaction of the EGF component in the EEP with its cell surface receptor [32,56].

In addition, the effect of EEP on cell migration was analyzed by comparing the scratch gap of different groups in a cell scratch assay (Figs. 3(b) and (c)). It was noted that the NIH/3T3 cells reached about 94% confluence at 24 h after treatment with EEP versus about 14% for the control group. Overall, the biological ability of EEP to promote cell proliferation and migration was verified. More importantly, the biological activities of EEP were well above those of EP, demonstrating the positive effect of the EGF ingredient. We further validated the biological functions of the EED adhesive by quantificationally estimating both NIH/3T3 and HSF cell viability by means of a CCK8 assay. The EED adhesive exhibited a marvelous capacity to promote cell proliferation, without a significant difference from the EGF gel group (Figs. 3(d) and (e)). Furthermore, after being treated with the extract of EED adhesive in serum-free DMEM for 24 h, the live NIH/3T3 cells showed a marked increase in green coloration, which was assessed visually using calcein–AM and PI double staining (Fig. 3(f)). The

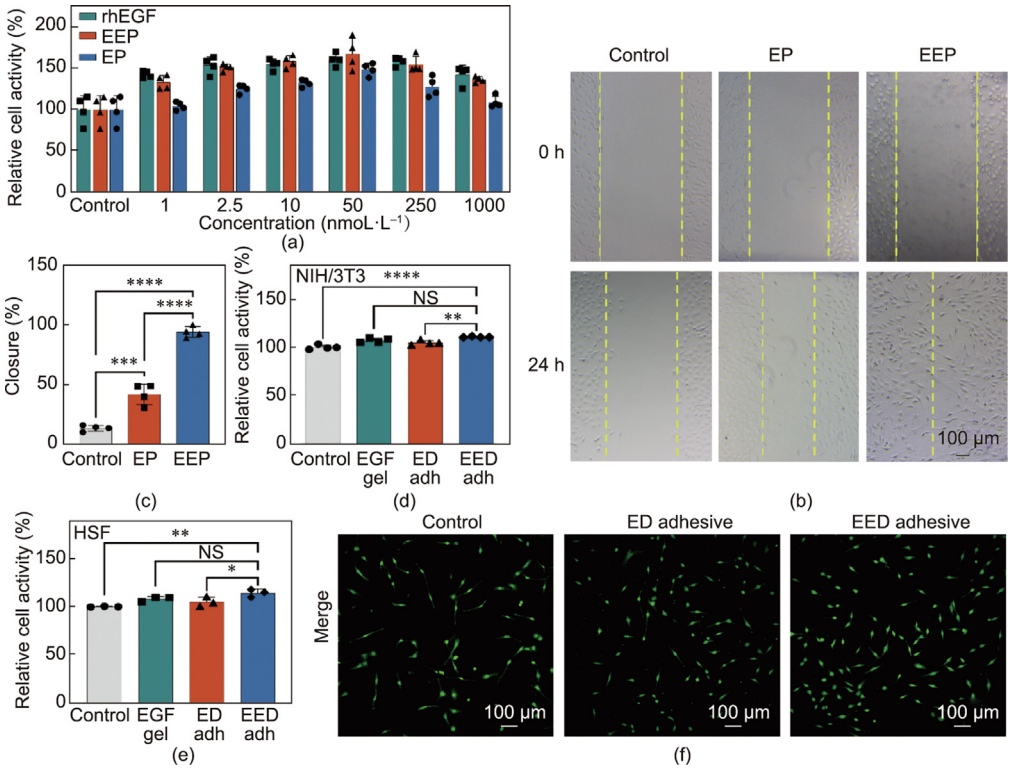

Fig. 3. The biological activities of the EEP and EED adhesive. (a) The ability of EEP to promote NIH/3T3 cell proliferation was evaluated by CCK8 assay at different concentrations (1 nmol·L^{-1}, 2.5 nmol·L^{-1}, 10 nmol·L^{-1}, 50 nmol·L^{-1}, 250 nmol·L^{-1}, and 1 μmol·L^{-1}). (b) Photographs and (c) quantitative analysis of EEP to promote NIH/3T3 cell migration. (d) The viability of NIH/3T3 cells treated with EED adhesive for 24 h was evaluated by CCK8 assay. NS: not significant. (e) HSF cell viability after treatment with the extract of the EED adhesive for 24 h was evaluated by CCK8 assay. Data are shown as mean ± SD (n = 3–4). One-way or two-way ANOVA was used to determine statistical significance. (f) Live/dead staining of NIH/3T3 cells after treatment with EED adhesive extract for 24 h; cellular state was observed with LSCM. adh: adhesive, $^{*}p < 0.05$, $^{**}p < 0.01$, $^{***}p < 0.001$, and $^{****}p < 0.0001$.

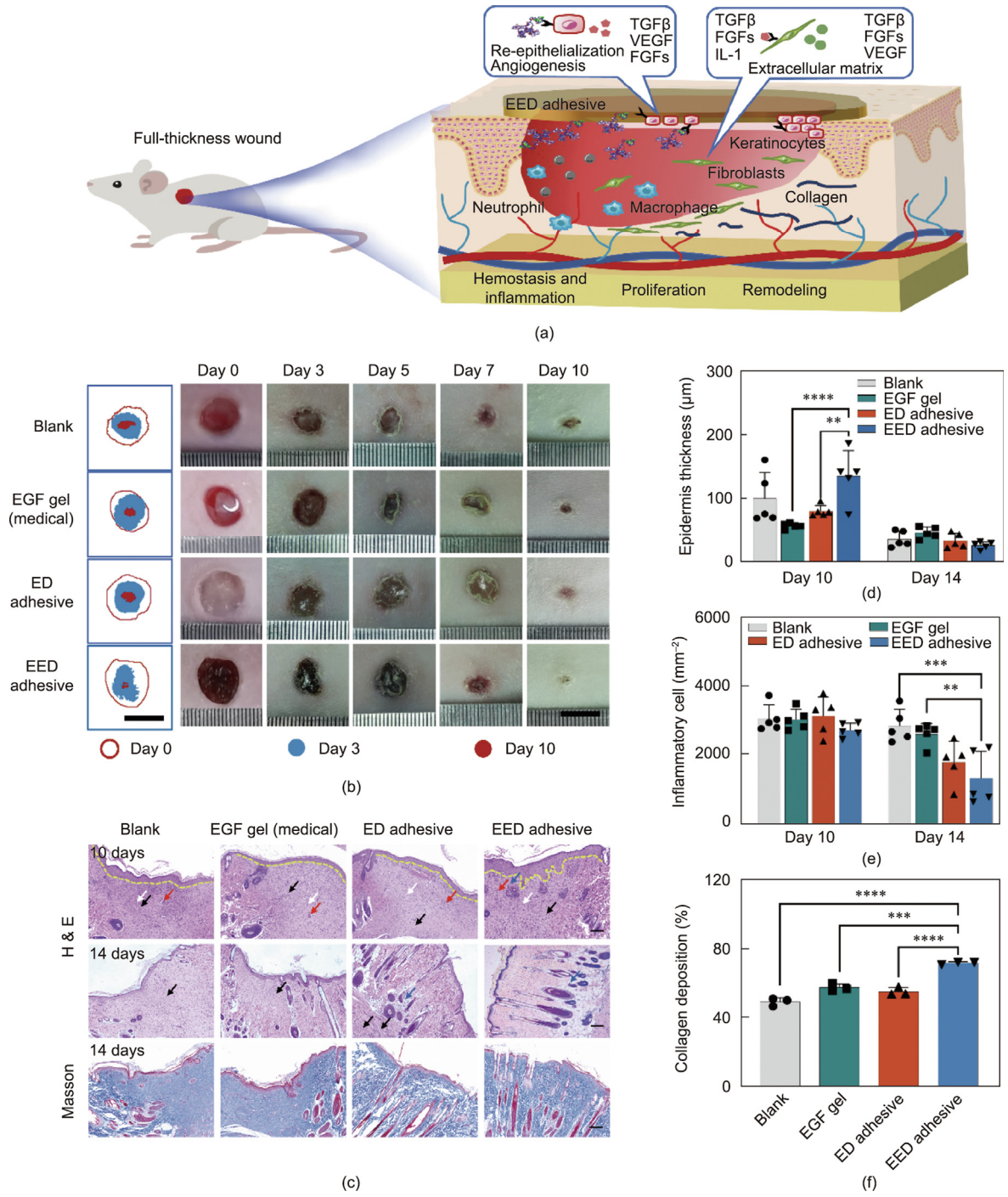

Fig. 4. Wound healing and histological analysis of the EED adhesive in full-thickness rat skin wound models. (a) Illustration of the wound healing mechanism of EED adhesive. (b) Photographs of wound healing on days 0, 3, 5, 7, and 10, respectively. A round full-thickness skin wound model was constructed on the back of the rats, and the wounds were treated with different adhesives, including blank (no treatment), commercial EGF gel, ED adhesive, and EED adhesive. The EED adhesive group clearly showed the best skin healing performance (scale bars: 1 cm). (c) Histological analysis of skin near the wound was performed using H&E staining (top) and Masson trichrome staining (bottom) (scale bars: 200 μm). (Demarcation line between new epidermis and dermis is marked by a yellow dotted line, inflammatory cells are marked by a black arrow, new small blood vessels are marked by a red arrow, new hair follicles are marked by a blue arrow, fibroblasts are marked by a white arrow.) (d, e) Quantitative analysis of (d) new epidermis thickness and (e) inflammatory cells in each group at days 10 and 14. (f) Collagen deposition in each group was quantitatively analyzed at day 14. Data are shown as mean ± SD. One-way or two-way ANOVA was used to determine statistical significance (**$p < 0.01$, ***$p < 0.001$, and ****$p < 0.0001$). TGFβ: transforming growth factor beta; VEGF: vascular endothelial growth factor; FGFs: fibroblast growth factor; IL-1: interleukin-1.

observational effect conformed well with the results of the quantitative data. In general, the above results demonstrated that the EED adhesive carries out biological functions in stimulating cell proliferation and migration. Thus, the EED adhesive is a promising biomedical material for accelerating skin healing.

Next, the adhesion/EGF healing combination effect of the EED adhesive was investigated in rat models with a full-thickness skin wound (Fig. 4(a)). The animals were randomly divided into four groups for different treatments, including blank, commercial EGF gel, ED adhesive, and EED adhesive. In all groups, the wounds were

photographed at different time points and analyzed statistically (Fig. 4(b); Fig. S12 in Appendix A). Notably, the EED adhesive exhibited prolonged adhesion on the skin model for up to 5 days, indicating its high bioavailability, which made it easy for it to exert a real-time pro-healing performance during wound contraction. On day 10, the wounds in the EED adhesive group showed near-perfect closure, while significant defects were observed in the other groups. Although the difference in healing rates between all groups decreased in the later stages of healing, which might be ascribed to the effect of endogenous EGF [33], the EED adhesive group still demonstrated extraordinary skin healing efficiency (98.7%) (Fig. S12(a)). Furthermore, larger scars were observed in the blank group with a scar area of 6% on day 14, which was almost twice that of the EED adhesive group (Fig. S12(b)). In brief, the EED adhesive has a positive effect on the wound healing process.

To investigate the skin regeneration process, a histological analysis was performed with H&E and Masson trichrome. Representative H&E results for four treatment conditions are shown in Fig. 4(c) and Fig. S13 in Appendix A. Compared with other treatment groups, the tissue in the EED adhesive group showed the narrowest area of damage (black dashed line) and well-formed connective tissue on day 10, indicating significantly faster neo-epidermal migration, which was consistent with the macroscopic observations. From the local magnification of the damaged area, it was found that the epidermis thickness in the EED adhesive group reached (136.5 ± 35.8) μm on day 10, which was higher than that in the other three groups, and eventually reached (27.6 ± 5.3) μm on day 14, which was comparable to normal skin (Fig. 4(d)). These findings are consistent with the fact that the epidermis thickness exhibits a process from thin to thicker, then gradually gets thinner, and finally approaches normal skin thickness during skin wound regeneration [57]. The above phenomena confirmed the excellent skin remodeling properties of the EED adhesive, which benefited from the biological activities that stimulated the proliferation and migration of keratinocytes and fibroblasts (Fig. 4(a)). Notably, on day 14, the inflammatory response vanished and a complete skin structure formed in the EED adhesive group. In stark contrast, there were still significant inflammatory cells and immature tissues in the blank and EGF gel groups, and slight infiltration of inflammatory cells in the ED adhesive group (black arrows) (Fig. 4(c)). The inflammatory cells of the four groups were analyzed quantitatively, from which it was seen that the EED adhesive had extraordinary healing performance, with minimal inflammation response (Fig. 4(e)). These phenomena are mainly attributed to the biological function of ELP directly and EGF indirectly reducing the inflammatory response [22,32,58].

Masson trichrome staining was executed for the assessment of collagen deposition. Among these groups, only the EED adhesive group showed well-aligned collagen and skin appendages (hair follicles, glands, etc.). In contrast, collagen was sparse in the ED adhesive group, and no mature granulation tissue was spotted in either the blank or EGF gel groups (Figs. 4(c) and S13). Consistent with the qualitative results, the percentage of collagen deposition in the EED adhesive group was 72%, which was statistically higher than that in other groups, indicating that the EED adhesive facilitated collagen deposition (Fig. 4(f)).

Based on these results, we propose that the EED adhesive provides a stable platform encapsulating EGF as an ingredient, exhibiting exceptional adhesion properties. Moreover, due to the immiscibility of the coacervate, the EED adhesive can effectively repel interfacial water and come into close contact with irregular surfaces, thus contributing to the action of the bioactive component EGF [59,60]. During wound healing, EGF binds to the EGF receptor and then initiates signaling cascades, thereby stimulating fibroblast and keratinocyte proliferation, and ultimately facilitating epithelialization, angiogenesis, and collagen deposition [61–63]. As a result, EED adhesive can realize real-time skin healing *in situ*, indicating its great potential in biomedical fields.

4. Conclusion

We developed an ECM-derived bioadhesive for *in situ* real-time tissue repair by actively introducing biological components and rational design of the ensemble system. The assembled adhesive was fabricated by harnessing liquid–liquid phase separation driven by electrostatic complexation between a chimeric EGF, EP, and natural DNA. The EED adhesive exhibited exceptional adhesion on various substrates (glass, ceramic, aluminum, steel, etc.) and on soft tissues (liver, muscle, porcine skin, etc.). In particular, the adhesion strength reached a remarkable (18.9 ± 0.9) MPa on steel substrates, and the adhesion energy reached (40.0 ± 5.3) $J \cdot m^{-2}$ on pig skin, outperforming many reported adhesives. More importantly, the EED adhesive presented extraordinary hemostatic behavior, promoted cell proliferation and migration, remodeled the ECM, and accelerated *in situ* skin regeneration. The outstanding features of the EED adhesive, which include biocompatibility, robust adhesion, and remarkable biological functions, make this type of bioadhesive promising in biomedical adhesion/healing translations. Moreover, this unique fabrication strategy holds great potential in the design of next-generation functionalized bioadhesives for broader applications such as bioelectronics, wearable health systems and beyond.

Acknowledgments

This research was supported by the National Key Research and Development Program of China (2022YFA0913200 and 2021YFB3502300), the National Natural Science Foundation of China (22020102003, 22125701, 22277064, 82272161, 52222214, and 22107097), Beijing Municipal Science and Technology Commission (221100007422088), Beijing Nova Program (Z211100002121132), Beijing Natural Science Foundation (2222010), and Xiangfu Lab Research Project (XF012022C0200).

Compliance with ethics guidelines

Ming Li, Baimei Liu, Wei Xu, Lai Zhao, Zili Wang, Haonan He, Jingjing Li, Fan Wang, Chao Ma, Kai Liu, and Hongjie Zhang declare that they have no conflict of interest or financial conflicts to disclose.

Appendix A. Supplementary data

Supplementary data to this article can be found online at https://doi.org/10.1016/j.eng.2023.07.013.

References

[1] Taboada GM, Yang K, Pereira MJN, Liu SS, Hu Y, Karp JM, et al. Overcoming the translational barriers of tissue adhesives. Nat Rev Mater 2020;5(4):310–29.
[2] Zhu J, Jin Q, Zhao H, Zhu W, Liu Z, Chen Q. Reactive oxygen species scavenging sutures for enhanced wound sealing and repair. Small Struct 2021;2(7):2100002.
[3] Ouyang J, Ji X, Zhang X, Feng C, Tang Z, Kong N, et al. *In situ* sprayed NIR-responsive, analgesic black phosphorus-based gel for diabetic ulcer treatment. Proc Natl Acad Sci USA 2020;117(46):28667–77.
[4] Chen X, Zhang J, Chen G, Xue Y, Zhang J, Liang X, et al. Hydrogel bioadhesives with extreme acid-tolerance for gastric perforation repairing. Adv Funct Mater 2022;32(29):2202285.
[5] Shirzaei Sani E, Kheirkhah A, Rana D, Sun Z, Foulsham W, Sheikhi A, et al. Sutureless repair of corneal injuries using naturally derived bioadhesive hydrogels. Sci Adv 2019;5(3):eaav1281.
[6] Nam S, Mooney D. Polymeric tissue adhesives. Chem Rev 2021;121(18):11336–84.

[7] Pinnaratip R, Bhuiyan MSA, Meyers K, Rajachar RM, Lee BP. Multifunctional biomedical adhesives. Adv Healthc Mater 2019;8(11):1801568.
[8] Balcioglu S, Gurses C, Ozcan I, Yildiz A, Koytepe S, Parlakpinar H, et al. Photocrosslinkable gelatin/collagen based bioinspired polyurethane-acrylate bone adhesives with biocompatibility and biodegradability. Int J Biol Macromol 2021;192:1344–56.
[9] Gao J, Yu X, Wang X, He Y, Ding J. Biomaterial-related cell microenvironment in tissue engineering and regenerative medicine. Engineering 2022;13:31–45.
[10] Feng C, Ouyang J, Tang Z, Kong N, Liu Y, Fu L, et al. Germanene-based theranostic materials for surgical adjuvant treatment: inhibiting tumor recurrence and wound infection. Matter 2020;3(1):127–44.
[11] Wang X, Tang M. Bioceramic materials with ion-mediated multifunctionality for wound healing. Smart Med 2022;1(1):e20220032.
[12] Bal-Ozturk A, Cecen B, Avci-Adali M, Topkaya SN, Alarcin E, Yasayan G, et al. Tissue adhesives: from research to clinical translation. Nano Today 2021;36:101049.
[13] Bouten PJM, Zonjee M, Bender J, Yauw STK, Van Goor H, Van Hest JCM, et al. The chemistry of tissue adhesive materials. Prog Polym Sci 2014;39(7):1375–405.
[14] Hofman AH, Van Hees IA, Yang J, Kamperman M. Bioinspired underwater adhesives by using the supramolecular toolbox. Adv Mater 2018;30(19):1704640.
[15] Zhao Q, Lee DW, Ahn BK, Seo S, Kaufman Y, Israelachvili JN, et al. Underwater contact adhesion and microarchitecture in polyelectrolyte complexes actuated by solvent exchange. Nat Mater 2016;15(4):407–12.
[16] Sun J, Chen J, Liu K, Zeng H. Mechanically strong proteinaceous fibers: engineered fabrication by microfluidics. Engineering 2021;7(5):615–23.
[17] Chang R, Yan X. Supramolecular immunotherapy of cancer based on the self-assembling peptide design. Small Struct 2020;1(2):2000068.
[18] Wang B, Chen H, Liu T, Shi S, Russell TP. Host–guest molecular recognition at liquid–liquid interfaces. Engineering 2021;7(5):603–14.
[19] Sun J, Zhang J, Zhao L, Wan S, Wu B, Ma C, et al. Contribution of hydrogen-bond nanoarchitectonics to switchable photothermal–mechanical properties of bioinorganic fibers. CCS Chem 2023;5(5):1242–50.
[20] Li J, Sun Y, Liang Y, Ma J, Li B, Ma C, et al. Extracellular elastin molecule modulates Alzheimer's aβ dynamics *in vitro* and *in vivo* by affecting microglial activities. CCS Chem 2021;3(7):1830–7.
[21] Sun J, Han J, Wang F, Liu K, Zhang H. Bioengineered protein-based adhesives for biomedical applications. Chemistry 2022;28(1):e202102902.
[22] Ma C, Sun J, Li B, Feng Y, Sun Y, Xiang L, et al. Ultra-strong bio-glue from genetically engineered polypeptides. Nat Commun 2021;12(1):3613.
[23] Brennan MJ, Kilbride BF, Wilker JJ, Liu JC. A bioinspired elastin-based protein for a cytocompatible underwater adhesive. Biomaterials 2017;124:116–25.
[24] Su J, Liu B, He H, Ma C, Wei B, Li M, et al. Engineering high strength and super-toughness of unfolded structural proteins and their extraordinary anti-adhesion performance for abdominal hernia repair. Adv Mater 2022;34(19):2200842.
[25] Wei Z, Sun J, Lu S, Liu Y, Wang B, Zhao L, et al. An engineered protein–Au bioplaster for efficient skin tumor therapy. Adv Mater 2022;34(16):2110062.
[26] Zhang Z, Zhou J, Liu C, Zhang J, Shibata Y, Kong N, et al. Emerging biomimetic nanotechnology in orthopedic diseases: progress, challenges, and opportunities. Trends Chem 2022;4(5):420–36.
[27] Zhou J, Zhang Z, Joseph J, Zhang X, Ferdows BE, Patel DN, et al. Biomaterials and nanomedicine for bone regeneration: progress and future prospects. Exploration 2021;1(2):20210011.
[28] Zhang X, Li L, Ouyang J, Zhang L, Xue J, Zhang H, et al. Electroactive electrospun nanofibers for tissue engineering. Nano Today 2021;39:101196.
[29] Li L, Zhang X, Zhou J, Zhang L, Xue J, Tao W, et al. Non-invasive thermal therapy for tissue engineering and regenerative medicine. Small 2022;18(36):2107705.
[30] Shan J, Che J, Song C, Zhao Y. Emerging antibacterial nanozymes for wound healing. Smart Med 2023;2(3):e20220025.
[31] Ren Y, Zhang Y, Liu Y, Wu Q, Hu HG, Li J, et al. Highly reliable and efficient encoding systems for hexadecimal polypeptide-based data storage. Fundam Res 2023;3(2):298–304.
[32] Kim H, Kong WH, Seong KY, Sung DK, Jeong H, Kim JK, et al. Hyaluronate–epidermal growth factor conjugate for skin wound healing and regeneration. Biomacromolecules 2016;17(11):3694–705.
[33] Shao M, Fan Y, Zhang K, Hu Y, Xu FJ. One nanosystem with potent antibacterial and gene-delivery performances accelerates infected wound healing. Nano Today 2021;39:101224.
[34] Zhao W, Li Y, Zhang X, Zhang R, Hu Y, Boyer C, et al. Photo-responsive supramolecular hyaluronic acid hydrogels for accelerated wound healing. J Control Release 2020;323:24–35.
[35] Sun J, Xiao L, Li B, Zhao K, Wang Z, Zhou Y, et al. Genetically engineered polypeptide adhesive coacervates for surgical applications. Angew Chem Int Ed 2021;60(44):23687–94.
[36] Wan S, Cheng W, Li J, Wang F, Xing X, Sun J, et al. Biological composite fibers with extraordinary mechanical strength and toughness mediated by multiple intermolecular interacting networks. Nano Res 2022;15(10):9192–8.
[37] Xiao L, Wang Z, Sun Y, Li B, Wu B, Ma C, et al. An artificial phase-transitional underwater bioglue with robust and switchable adhesion performance. Angew Chem Int Ed 2021;60(21):12082–9.
[38] Li J, Celiz AD, Yang J, Yang Q, Wamala I, Whyte W, et al. Tough adhesives for diverse wet surfaces. Science 2017;357:378–81.
[39] Xi S, Tian F, Wei G, He X, Shang Y, Ju Y, et al. Reversible dendritic-crystal-reinforced polymer gel for bioinspired adaptable adhesive. Adv Mater 2021;33(40):2103174.
[40] Harris TI, Gaztambide DA, Day BA, Brock CL, Ruben AL, Jones JA, et al. Sticky situation: an investigation of robust aqueous-based recombinant spider silk protein coatings and adhesives. Biomacromolecules 2016;17(11):3761–72.
[41] Annabi N, Zhang YN, Assmann A, Sani ES, Cheng G, Lassaletta AD, et al. Engineering a highly elastic human protein-based sealant for surgical applications. Sci Transl Med 2017;9(410):eaai7466.
[42] Zhang D, Xu Z, Li H, Fan C, Cui C, Wu T, et al. Fabrication of strong hydrogen-bonding induced coacervate adhesive hydrogels with antibacterial and hemostatic activities. Biomater Sci 2020;8(5):1455–63.
[43] Zhang Q, Shi CY, Qu DH, Long YT, Feringa BL, Tian H. Exploring a naturally tailored small molecule for stretchable, self-healing, and adhesive supramolecular polymers. Sci Adv 2018;4(7):eaat8192.
[44] Xu J, Li X, Li J, Li X, Li B, Wang Y, et al. Wet and functional adhesives from one-step aqueous self-assembly of natural amino acids and polyoxometalates. Angew Chem Int Ed 2017;56(30):8731–5.
[45] Wonderly WR, Cristiani TR, Cunha KC, Degen GD, Shea JE, Waite JH. Dueling backbones: comparing peptoid and peptide analogues of a mussel adhesive protein. Macromolecules 2020;53(16):6767–79.
[46] Liu X, Zhang Q, Gao Z, Hou R, Gao G. Bioinspired adhesive hydrogel driven by adenine and thymine. ACS Appl Mater Interfaces 2017;9(20):17645–52.
[47] Meng Z, Liu Q, Zhang Y, Sun J, Yang C, Li H, et al. Highly stiff and stretchable DNA liquid crystalline organogels with super plasticity, ultrafast self-healing, and magnetic response behaviors. Adv Mater 2022;34(3):2106208.
[48] Li F, Tang J, Geng J, Luo D, Yang D. Polymeric DNA hydrogel: design, synthesis and applications. Prog Polym Sci 2019;98:101163.
[49] Zhao X, Liang Y, Huang Y, He J, Han Y, Guo B. Physical double-network hydrogel adhesives with rapid shape adaptability, fast self-healing, antioxidant and NIR/pH stimulus-responsiveness for multidrug-resistant bacterial infection and removable wound dressing. Adv Funct Mater 2020;30(17):1910748.
[50] Chen W, Wang R, Xu T, Ma X, Yao Z, Chi B, et al. A mussel-inspired poly(γ-glutamic acid) tissue adhesive with high wet strength for wound closure. J Mater Chem B 2017;5(28):5668–78.
[51] Pei X, Zhang H, Zhou Y, Zhou L, Fu J. Stretchable, self-healing and tissue-adhesive zwitterionic hydrogels as strain sensors for wireless monitoring of organ motions. Mater Horiz 2020;7(7):1872–82.
[52] Fan H, Gong JP. Bioinspired underwater adhesives. Adv Mater 2021;33(44):2102983.
[53] Wei W, Tan Y, Martinez Rodriguez NR, Yu J, Israelachvili JN, Waite JH. A mussel-derived one component adhesive coacervate. Acta Biomater 2014;10(4):1663–70.
[54] Filippidi E, Cristiani TR, Eisenbach CD, Waite JH, Israelachvili JN, Ahn BK, et al. Toughening elastomers using mussel-inspired iron-catechol complexes. Science 2017;358:502–5.
[55] Lang N, Pereira MJ, Lee Y, Friehs I, Vasilyev NV, Feins EN, et al. A blood-resistant surgical glue for minimally invasive repair of vessels and heart defects. Sci Transl Med 2014;6(218):218ra6.
[56] Choi JK, Jang JH, Jang WH, Kim J, Bae IH, Bae J, et al. The effect of epidermal growth factor (EGF) conjugated with low-molecular-weight protamine (LMWP) on wound healing of the skin. Biomaterials 2012;33(33):8579–90.
[57] Xi Y, Ge J, Guo Y, Lei B, Ma PX. Biomimetic elastomeric polypeptide-based nanofibrous matrix for overcoming multidrug-resistant bacteria and enhancing full-thickness wound healing/skin regeneration. ACS Nano 2018;12(11):10772–84.
[58] Hu B, Gao M, Boakye-Yiadom KO, Ho W, Yu W, Xu X, et al. An intrinsically bioactive hydrogel with on-demand drug release behaviors for diabetic wound healing. Bioact Mater 2021;6(12):4592–606.
[59] Peng X, Li Y, Li T, Li Y, Deng Y, Xie X, et al. Coacervate-derived hydrogel with effective water repulsion and robust underwater bioadhesion promotes wound healing. Adv Sci 2022;9(31):2203890.
[60] Peng Q, Chen J, Zeng Z, Wang T, Xiang L, Peng X, et al. Adhesive coacervates driven by hydrogen-bonding interaction. Small 2020;16(43):2004132.
[61] Koehler J, Brandl FP, Goepferich AM. Hydrogel wound dressings for bioactive treatment of acute and chronic wounds. Eur Polym J 2018;100:1–11.
[62] Ying R, Huang WC, Mao X. Synthesis of agarose-based multistimuli-responsive hydrogel dressing for accelerated wound healing. ACS Biomater Sci Eng 2022;8(1):293–302.
[63] Jiang F, Chi Z, Ding Y, Quan M, Tian Y, Shi J, et al. Wound dressing hydrogel of *Enteromorpha prolifera* polysaccharide–polyacrylamide composite: a facile transformation of marine blooming into biomedical material. ACS Appl Mater Interfaces 2021;13(12):14530–42.